Discovery of ^{18}F-JK-PSMA-7, a PET Probe for the Detection of Small PSMA-Positive Lesions

Boris D. Zlatopolskiy*[1–3], Heike Endepols*[1,2,4], Philipp Krapf[1,2], Mehrab Guliyev[1], Elizaveta A. Urusova[1,2], Raphael Richarz[1,2], Melanie Hohberg[4], Markus Dietlein[4], Alexander Drzezga[4], and Bernd Neumaier[1–3]

[1]Institute of Radiochemistry and Experimental Molecular Imaging, University Hospital of Cologne, Cologne, Germany; [2]Institute of Neuroscience and Medicine, INM-5: Nuclear Chemistry, Forschungszentrum Jülich GmbH, Jülich, Germany; [3]Max Planck Institute for Metabolism Research, Cologne, Germany; and [4]Department of Nuclear Medicine, University Hospital of Cologne, Cologne, Germany

Prostate-specific membrane antigen (PSMA), expressed by most prostate carcinomas (PCa), is a promising target for PCa imaging. The application of PSMA-specific ^{18}F-labeled PET probes such as ^{18}F-DCFPyL and ^{18}F-PSMA-1007 considerably improved the accuracy of PCa tumor detection. However, there remains a need for further improvements in sensitivity and specificity. The aim of this study was the development of highly selective and specific PSMA probes with enhanced imaging properties, in comparison with ^{18}F-DCFPyL, ^{18}F-PSMA-1007, and ^{68}Ga-PSMA-11. **Methods:** Eight novel ^{18}F-labeled PSMA ligands were prepared. Their cellular uptake in PSMA-positive LNCaP C4–2 and PSMA-negative PC-3 cells was compared with that of ^{18}F-DCFPyL. The most promising candidates were additionally evaluated by small-animal PET in healthy rats using PSMA-positive peripheral ganglia as a model for small PCa lesions. PET images of the ligand with the best outcome, ^{18}F-JK-PSMA-7, were compared with those of ^{18}F-DCFPyL, ^{18}F-PSMA-1007, and ^{68}Ga-PSMA-11 with respect to key image-quality parameters for the time frame 60–120 min. **Results:** Compared with ^{18}F-DCFPyL, ^{18}F-JK-PSMA-7 demonstrated increased PSMA-specific cellular uptake. Although target-to-background ratios of ^{18}F-DCFPyL and ^{18}F-PSMA-1007 were comparable, this parameter was higher for ^{18}F-JK-PSMA-7 and lower for ^{68}Ga-PSMA-11. Image acutance was significantly higher for ^{18}F-JK-PSMA-7 and ^{18}F-PSMA-1007 than for ^{18}F-DCFPyL and ^{68}Ga-PSMA-11. Image resolution was similar for all 4 tracers. ^{18}F-PSMA-1007 demonstrated significantly higher blood protein binding and bone uptake than the other tracers. **Conclusion:** ^{18}F-JK-PSMA-7 is a promising candidate for high-quality visualization of small PSMA-positive lesions. Excellent preclinical imaging properties justify further preclinical and clinical studies of this tracer.

Key Words: prostate carcinoma; PSMA; radiofluorination; positron emission tomography; imaging; preclinical model

J Nucl Med 2019; 60:817–823
DOI: 10.2967/jnumed.118.218495

Prostate-specific membrane antigen (PSMA) is expressed by most prostate carcinomas (PCas). The level of PSMA expression correlates with tumor aggressiveness (*1*). Consequently, PSMA represents an excellent molecular target for PCa imaging. ^{68}Ga-PSMA PET is already widely used for PCa diagnostics (*2*). However, the growing demand for PSMA imaging agents stimulated the development of ^{18}F-labeled PSMA ligands. Among them, ^{18}F-DCFPyL (*3*) has already been evaluated in several clinical centers (*4–10*). Nevertheless, some limitations remain with respect to pharmacokinetics and detection rates in patients with very low prostate-specific antigen values (<1 ng/mL). Thus, there is still room for the development of more sensitive PSMA-specific probes. Importantly, availability on a preparative scale using efficient current good manufacturing practices amenable to automation is a prerequisite for its clinical application. Here, we present 8 novel radiofluorinated candidates (Fig. 1) together with their in vitro and in vivo evaluation.

MATERIALS AND METHODS

Preparation of PSMA-Specific PET Probes

^{68}Ga-PSMA-11 and ^{18}F-PSMA-1007 were synthesized according to Eder et al. (*11*) and Cardinale et al. (*12*), respectively. ^{18}F-DCFPyL (^{18}F-**2**), ^{18}F-JK-PSMA-7–9 (^{18}F-**4**–**6**), and ^{18}F-JK-PSMA-11–13 (^{18}F-**8**–**10**) were prepared using the minimalist approach (*13*) according to the modified protocol of Neumaier et al. (*14*) (Fig. 2; Supplemental Fig. 1 [supplemental materials are available at http://jnm.snmjournals.org]). The manual synthesis and automated production of ^{18}F-JK-PSMA-7 on an FXNPro module (GE Healthcare) are shown in Supplemental Figure 2. ^{18}F-JK-PSMA-10 (^{18}F-**7**) was prepared applying the minimalist protocol to the procedure proposed for the preparation of ^{18}F-DCFPyL by Bouvet et al. (*15*) and Ravert et al. (*16*). ^{18}F-JK-PSMA-14 (^{18}F-**11**) was prepared as described elsewhere (*17*). The preparation of intermediates, precursors for radiolabeling, and reference compounds is shown in the supplemental data or was previously published (*18–22*).

Cellular Uptake Studies

Cells were cultivated as described in the supplemental data. The PET tracer was added to the cells (100–150 kBq/well, 3 wells per tracer) and incubated at 37°C for 2 and 4 h. 2-(phosphonomethyl) pentanedioic acid (100 μm/well) was used for blocking studies. Cells were trypsinized, harvested, and measured in a γ-counter (Wizard 1470; PerkinElmer), and percentage uptake per 10^5 cells was calculated. Uptake of ^{18}F-DCFPyL was always measured in parallel. Cellular

Received Jul. 25, 2018; revision accepted Oct. 22, 2018.
For correspondence or reprints contact: Bernd Neumaier, Institute of Neuroscience and Medicine, INM-5: Nuclear Chemistry, Forschungszentrum Jülich GmbH, Wilhelm-Johnen-Straße, 52425 Jülich, Germany.
E-mail: b.neumaier@fz-juelich.de
*Contributed equally to this work.
Published online Nov. 2, 2018.

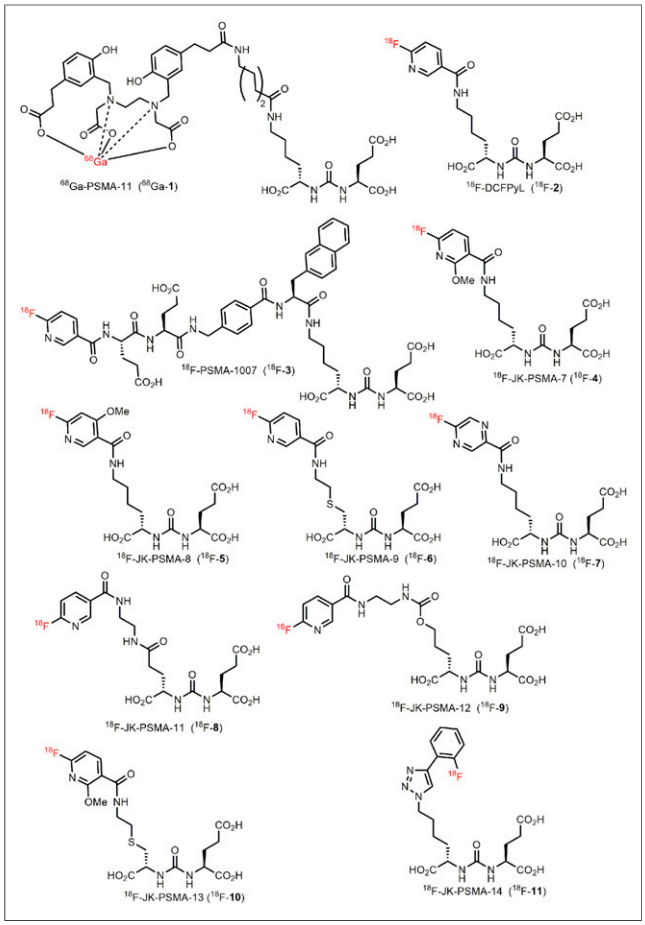

FIGURE 1. Previously known PSMA-specific PET tracers (^{68}Ga-**1,** ^{18}F-**2,** and ^{18}F-**3**) and emerging probes (^{18}F-JK-**4**-**11**) investigated in this study.

uptake values were compared using 2-way ANOVA followed by the Sidak multiple-comparison test ($P < 0.05$).

PET Evaluation of PSMA-Specific Tracers in Healthy Rats

Healthy Long Evans rats (11 male, 2 female; 250–530 g) were used for this study. Rats were housed in groups of 2–4 animals under controlled conditions (22°C ± 1°C and 55% ± 5% relative humidity) and an inversed 12-h light/dark schedule (lights on 8:30 PM–8:30 AM). Rats had free access to water and food. Experiments were performed in accordance with European Union directive 2010/63/EU for animal experiments and were approved by regional authorities (Ministry for Environment, North Rhine-Westphalia).

Before PET measurements, animals were anesthetized (initially, 5% isoflurane in O_2/air (3:7); then, reduction to 2%), and a catheter for tracer injection was inserted into the lateral tail vein. Dynamic PET scans in list mode were performed using a Focus 220 small-animal PET scanner (CTI-Siemens). Data acquisition started with tracer injection (17–77 MBq in 0.5 mL), continued for 120 min, and was followed by a 10-min transmission scan using a ^{57}Co point source. For blocking studies, the PSMA inhibitor 2-(phosphonomethyl)pentanedioic acid (23 mg/kg) was injected together with the radiotracer. Body temperature was maintained at 37°C by a feedback-controlled system. Images were reconstructed using an iterative 3-dimensional ordered-subsets expectation maximization algorithm followed by a maximum a posteriori procedure (*23*) resulting in voxel sizes of 0.38 × 0.38 × 0.80 mm. The 120-min measurement was divided into different time frames (2 × 60 min or 4 × 30 min; for time–activity curves: 2 × 1 min, 2 × 2 min, 6 × 4 min, 18 × 5 min). Postprocessing and image analysis were performed with Vinci, version 4.72 (Max Planck Institute for Metabolism Research). Frames were Gauss-filtered (1 mm in full width at half maximum [FWHM]) and intensity-normalized to injected dose, corrected for body weight (SUV_{BW}). Tracer tissue accumulation was measured for the 60- to 120-min frame and compared among tracers using 1-way ANOVA followed by Dunnett multiple-comparisons testing.

Analysis of PET Image Quality

Target-to-Background Ratio (TBR). TBR describes the delineation of PSMA-positive ganglia against PSMA-negative background. Two elliptic volumes of interest were used: The first volume of interest (150 voxels) was placed over the superior cervical ganglion (SCG) and the second (1,600 voxels) over the neck region dorsal from the spinal cord. Volume of interest mean values were extracted, and the SCG/background ratio was calculated. TBR was first determined for candidate probes (^{18}F-JK-PSMA-7-11 and -13) and compared with ^{18}F-DCFPyL in the same animal for the time frame 60–120 min. The most promising candidate, ^{18}F-JK-PSMA-7 (56–63 MBq); its regioisomer, ^{18}F-JK-PSMA-8 (47–70 MBq); ^{18}F-DCFPyL (45–71 MBq); ^{18}F-PSMA-1007 (17–59 MBq); and ^{68}Ga-PSMA-11 (13–51 MBq) were evaluated in 3 animals each. ^{18}F-JK-PSMA-9-11 and -13 were not further evaluated.

Acutance. The image intensity of a PSMA-positive ganglion decreases gradually to background level, forming a slope that reflects the edge contrast or acutance. An 8-mm profile (1-pixel width) was placed over the middle of the SCG (diameter, ~3.5 mm) in the horizontal plane. The slope of the profile plot was determined by dividing the maximum height of the SCG profile (peak minus background) by its FWHM. The time frame used for this analysis was 60–120 min after injection.

Resolution. The dorsal root ganglia (DRG) are arranged in pairs along the spinal cord. The parameter "spatial resolution" describes how well the two ganglia of one pair can be separated from each other. A 12-mm profile was placed over the first cervical pair of DRG (ganglion diameter, ~2.5 mm; distance from center to center, ~4 mm) in

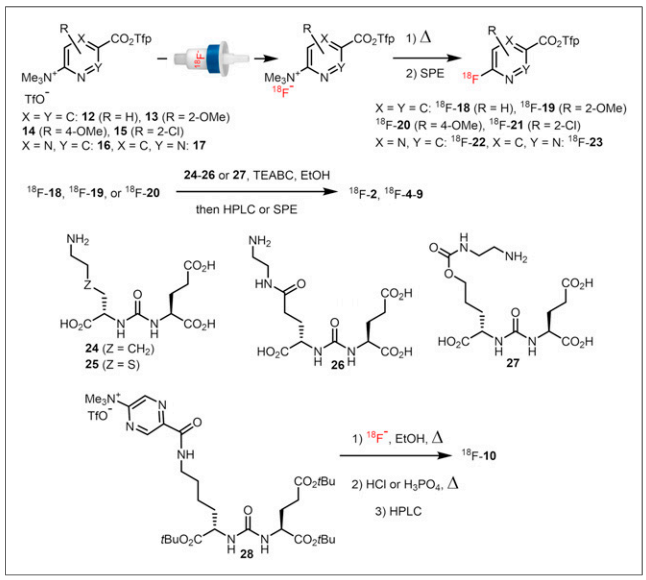

FIGURE 2. Preparation of ^{18}F-**2** and ^{18}F-**4**-**10**. TEABC = tetraethylammonium bicarbonate.

the horizontal plane. We used the formula commonly used in chromatography (*24*):

$$R = \frac{2(P1 - P2)}{1.7(FWHM1 + FWHM2)},$$

with R being resolution and P1–P2 the distance between peaks.

Image quality parameters were compared among tracers using 1-way ANOVA followed by Dunnett multiple-comparisons testing. In addition, TBRs were compared using 2-way ANOVA with the factors "tracer" and "frame," followed by Tukey multiple-comparisons testing. The time frame analyzed was 60–120 min after injection.

Patient PET/CT Scan

A first-in-human study with ^{18}F-JK-PSMA-7 was performed on a patient within the clinical workup. The patient had given his written informed consent for PET imaging and the scientific evaluation of his data. All procedures were performed in accordance with the Institutional Review Board and the regulations of the responsible local authorities (Bezirksregierung Köln).

RESULTS

Preparation of PET Probes

^{18}F-DCFPyL and the novel PET tracers, ^{18}F-JK-PSMA-7–9 and -11–13, were prepared by the acylation of ureas **24**–**27** with the appropriate ^{18}F-labeled active ester, ^{18}F-**18**–**20**, in anhydrous EtOH using Et_4NHCO_3 as a base and purified by solid-phase extraction or high-performance liquid chromatography (Fig. 2) (*14*). ^{18}F-**18**–**23** were synthesized by direct elution of ^{18}F-fluoride previously loaded onto an anion exchange resin with a solution of the corresponding radiolabeling precursor in a suitable solvent (EtOH, EtOH/MeCN/*t*BuOH, MeCN/*t*BuOH, or MeCN). Subsequently, the solution was heated to 40°C for 2–5 min (if pure EtOH was used for elution, it was preliminarily diluted with a MeCN/*t*BuOH mixture; in this case, the reaction time amounted to 15–20 min) and purified by solid-phase extraction. Using this protocol, ^{18}F-DCFPyL and ^{18}F-JK-PSMA-7–9 and -10–13 were prepared in 2 steps in non–decay-corrected radiochemical yields of 12%–25%. ^{18}F-**21**–**23** were insufficiently stable and defluorinated rapidly during purification (^{18}F-**22**) or the second reaction step (^{18}F-**21** and ^{18}F-**23**). Consequently, ^{18}F-**7** was prepared starting from **28** using a modified minimalist approach (*13*). ^{18}F-fluoride was eluted from the anion-exchange cartridge with a solution of **28** in EtOH, and the resulting solution was heated at 150°C for 20 min, affording the protected intermediate, which was purified by solid-phase extraction and deprotected using H_3PO_4 or HCl in aqueous MeCN at 45°C for 5 min. Finally, ^{18}F-JK-PSMA-10 was isolated by high-performance liquid chromatography in 3%–5% radiochemical yield.

Cellular Uptake Studies

All tested PET tracers showed a significantly increased uptake in LNCaP cells after 4 h compared with 2 h ($F_{1,34}$ = 8081; $P <$ 0.0001 for factor "time"; post hoc $P < 0.05$). In contrast, tracer uptake in PSMA-negative PC-3 cells was low (Supplemental Fig. 3; Supplemental Table 1). The PSMA specificity of tracer uptake in LNCaP C4-2 cells was confirmed by the inhibition with 2-(phosphonomethyl)pentanedioic acid.

Comparison between uptake in LNCaP C4-2 cells of ^{18}F-**4**–**11** in relation to that of ^{18}F-DCFPyL is shown in Figure 3. Only ^{18}F-JK-PSMA-7 exhibited a significantly higher cellular uptake than ^{18}F-DCFPyL after 2 h ($F_{7,38}$ = 1,136; $P <$ 0.0001 for factor "tracer"; post hoc $P < 0.05$). For all other tracers, uptake in LNCaP C4-2 cells after 2 h was significantly lower than that of ^{18}F-DCFPyL (Supplemental Table 2). After 4 h, cellular uptake of ^{18}F-JK-PSMA-7 in LNCaP C4-2 cells was also significantly higher, whereas uptake of ^{18}F-JK-PSMA-9 and -11 was comparable to that of ^{18}F-DCFPyL. All other tracers showed a significantly lower uptake after 4 h. Because of the low PSMA-specific cellular uptake, ^{18}F-JK-PSMA-12 and -14 were excluded from further studies.

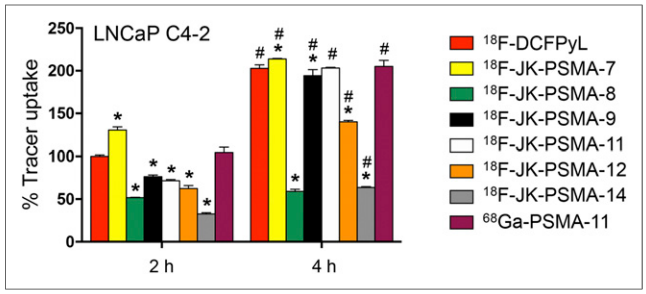

FIGURE 3. Tracer uptake in LNCaP C4-2 cells in relation to ^{18}F-DCFPyL. ^{18}F-DCFPyL uptake after 2 h was normalized to 100%. Only ^{18}F-JK-PSMA-7 shows higher uptake than ^{18}F-DCFPyL. *Significantly different from ^{18}F-DCFPyL at same time point. $F_{7,38}$ = 1,136; $P <$ 0.0001 for factor "tracer," post hoc $P < 0.05$. #Significantly higher than 2-h uptake of same tracer. $F_{1,38}$ = 6,981; $P < 0.0001$ for factor "time," post hoc $P < 0.05$.

Initial In Vivo Experiments

Stability toward defluorination, as well as the TBR of the PET tracers, was determined in healthy rats using small-animal PET. All tracers except ^{18}F-JK-PSMA-10 were sufficiently stable in vivo (Supplemental Figs. 4 and 5). TBR determined for the SCG was highest for ^{18}F-JK-PSMA-7, followed by ^{18}F-DCFPyL, ^{18}F-PSMA-1007, ^{18}F-JK-PSMA-8, and finally ^{68}Ga-PSMA-11 (Fig. 4B; Table 1). Analysis of four 30-min frames revealed that the TBR of ^{18}F-JK-PSMA-7 and ^{18}F-PSMA-1007 increased over time (Fig. 4C). Notably, ^{18}F-PSMA-1007 demonstrated the highest SCG accumulation (94.8 ± 19.6 SUV_{BW}). However, because of the high background radioactivity of 15.86 ± 1.68 SUV_{BW}, the TBR for this tracer was not higher than the TBR for ^{18}F-DCFPyL or ^{18}F-JK-PSMA-7. The TBR for ^{18}F-JK-PSMA-9 (4.0), ^{18}F-JK-PSMA-10 (2.1), ^{18}F-JK-PSMA-11 (2.6), and ^{18}F-JK-PSMA-13 (4.3) were determined once in the same animal (Supplemental Fig. 4). Because of insufficiently high TBR (<4.5), these tracers were not further evaluated.

Biodistribution and Biokinetics of ^{18}F-DCFPyL, ^{18}F-PSMA-1007, ^{18}F-JK-PSMA-7, ^{18}F-JK-PSMA-8, and ^{68}Ga-PSMA-11 in Healthy Rats

^{18}F-DCFPyL demonstrated a slow washout from all tissues (Supplemental Fig. 5A; Table 2), comparable to that of ^{18}F-JK-PSMA-7. Liver accumulation of ^{18}F-JK-PSMA-7 reached the maximal value of 302.1 ± 83.2 SUV_{BW} 24 min after injection (Supplemental Fig. 5B) and decreased to 119.3 ± 8.3 SUV_{BW}. This was still significantly higher than those for ^{18}F-JK-PSMA-8 and ^{18}F-PSMA-1007 ($F_{4,10}$ = 7.83, P = 0.0040; post hoc $P < 0.05$). Despite the very close structural similarity, the biodistribution data of ^{18}F-JK-PSMA-7 and ^{18}F-JK-PSMA-8 revealed significant differences. Bone uptake of ^{18}F-JK-PSMA-8 (19.2 ± 2.1 SUV_{BW}) was 6 times higher than background uptake and twice as high as SCG uptake (Table 2), indicating that defluorination took place

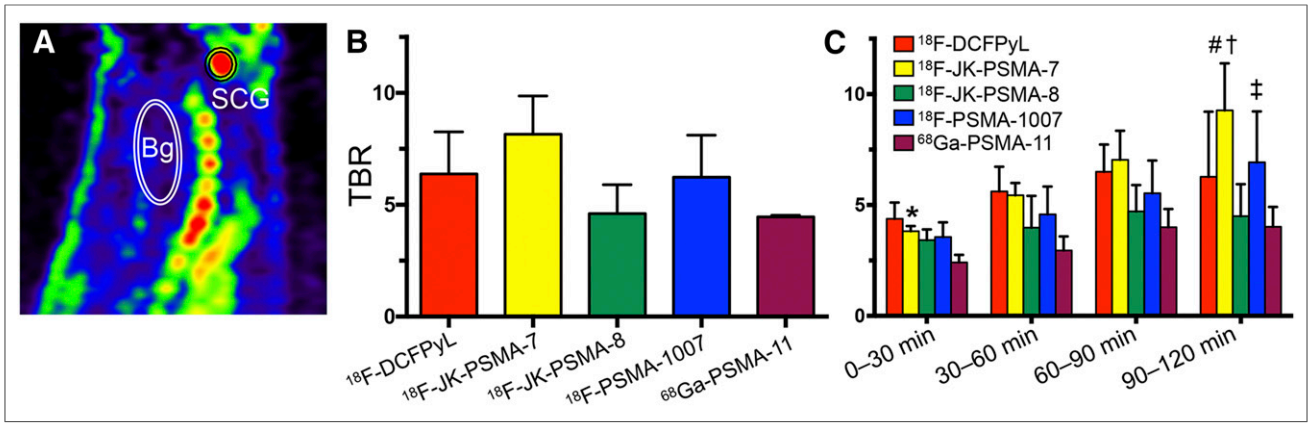

FIGURE 4. TBR of PSMA tracers. (A) Sagittal section of PSMA image with SCG and background (Bg) volumes of interest. (B) Graph showing that TBR (SCG/Bg) 60–120 min after injection did not significantly differ among groups ($F_{4,10} = 2.95$, $P = 0.0756$). (C) TBR analyzed for four 30-min frames. *TBE significantly higher for ^{18}F-JK-PSMA-7 than for ^{68}Ga-PSMA-11 ($F_{4,40} = 5.97$, $P = 0.0102$, for factor "tracer," post hoc $P < 0.05$). #TBR significantly higher for ^{18}F-JK-PSMA-7 than for ^{18}F-JK-PSMA-8 or ^{68}Ga-PSMA-11 ($P < 0.05$). TBR of ^{18}F-JK-PSMA-7 and ^{18}F-PSMA-1007 increased significantly over time ($F_{3,30} = 9.12$, $P = 0.0002$, for factor "frame"). †For ^{18}F-JK-PSMA-7, frame 4 was significantly different from frames 1 and 2 ($P < 0.05$). ‡For ^{18}F-PSMA-1007, frame 4 was significantly different from frame 1 ($P < 0.05$).

(Supplemental Fig. 5C). Accordingly, tracer uptake in the DRG was completely obscured. Compared with the other tracers, ^{18}F-PSMA-1007 demonstrated a significantly higher accumulation (post hoc $P < 0.05$) in all tissues, including SCG, salivary gland, and bone, but not in the liver (Table 2). The DRG were clearly visible, and the SCG signal plateaued with no further washout after 1 h after injection (Supplemental Fig. 5D). Bone accumulation of ^{18}F-PSMA-1007 was much higher than that of any other tracer, even compared with ^{18}F-JK-PSMA-8. However, tracer biodistribution did not provide evidence for significant defluorination, since bone uptake was almost 3 times lower than SCG uptake and only twice as high as background. Uptake of ^{68}Ga-PSMA-11 in evaluated tissues was lower than that of ^{18}F-PSMA-1007 but higher than that of the other tracers (Table 2). Measurement of blood radioactivity in the lumen of the left ventricle revealed a significantly higher value for ^{18}F-PSMA-1007 and for ^{68}Ga-PSMA-11 than for the other tracers (8.61–16.28 SUV_{BW}; $F_{3,8} = 53.53$, $P < 0.0001$; post hoc $P < 0.05$) (Table 2; Supplemental Fig. 6).

Comparison of Image Quality

Acutance measured in the SCG was significantly higher for ^{18}F-JK-PSMA-7 and ^{18}F-PSMA-1007 than for ^{18}F-DCFPyL and ^{68}Ga-PSMA-11 ($F_{4,10} = 12.77$, $P = 0.0006$; post hoc $P < 0.05$; Fig. 5; Table 1). Spatial resolution, measured for the apical pair of cervical DRG, was significantly higher for ^{18}F-JK-PSMA-7 than for ^{18}F-JK-PSMA-8 ($F_{4,10} = 3.80$, $P = 0.0396$; post hoc $P < 0.05$; Fig. 6; Table 1).

TABLE 1
Comparison of Quality of PET Images Obtained with Different Tracers (60–120 Minutes After Injection, $n = 3$)

Tracer	Acutance	Resolution	TBR
^{18}F-DCFPyL	0.019 ± 0.008	1.002 ± 0.141	6.38 ± 1.87
^{18}F-JK-PSMA-7	0.075 ± 0.027*	1.095 ± 0.042†	8.15 ± 1.71
^{18}F-JK-PSMA-8	0.021 ± 0.005	0.800 ± 0.032	4.60 ± 1.30
^{18}F-PSMA-1007	0.097 ± 0.025*	0.924 ± 0.074	6.23 ± 1.88
^{68}Ga-PSMA-11	0.024 ± 0.009	0.892 ± 0.146	4.46 ± 0.08

*Significantly higher than ^{18}F-DCFPyL, ^{18}F-JK-PSMA-8, and ^{68}Ga-PSMA-11 ($F_{4,10} = 12.77$, $P = 0.0006$; post hoc $P < 0.05$).
†Significantly higher than ^{18}F-JK-PSMA-8 ($F_{4,10} = 3.80$, $P = 0.0396$; post hoc $P < 0.05$).

^{18}F-JK-PSMA-7 in a Patient with PCa Recurrence

A first-in-human study was conducted with ^{18}F-JK-PSMA-7 (Fig. 7). A 64-y-old patient with an elevated prostate-specific antigen level (130 ng/mL) was referred for PSMA PET/CT before further treatment. A ^{18}F-JK-PSMA-7 PET scan demonstrated tracer accumulation in the prostate, skeletal lesions, and pelvic lymph nodes.

DISCUSSION

^{18}F-DCFPyL, ^{18}F-JK-PSMA-7–9, and ^{18}F-JK-PSMA-11–13 were prepared using a 2-step procedure outlined in Figure 2. This modular approach enabled the application of the same building blocks for the synthesis of different radiotracers. ^{18}F-labeled active esters ^{18}F-**18**–**23** were obtained in radiochemical yields of up to 85% within 8–20 min using only ^{18}F-fluoride and the corresponding labeling precursor without any evaporation steps. The acylation step worked well only in anhydrous EtOH. If the reaction was performed in aprotic or aqueous medium, much lower radiochemical conversions (0%–15%) were observed. The final purification by solid-phase extraction or high-performance liquid chromatography afforded tracers in good radiochemical yields (12%–25%, non–decay-corrected) and excellent radiochemical purity (>98%). The simplicity of the preparation procedure enabled a straightforward transfer to synthesis modules. Because of the insufficient stability of ^{18}F-**20**, ^{18}F-JK-PSMA-13 was prepared from the corresponding protected precursor, **28**. The electron-poor nature of the pyridazine ring allowed—for the first time, to our knowledge—high-yielding SNAr radiofluorination in pure primary alcohols such as EtOH in more than 90% radiochemical conversions. Unfortunately, it also caused substantial decomposition during the deprotection step.

Next, we started the biologic evaluation of the novel radiotracers. Their PSMA-specific cellular uptake was compared with that of ^{18}F-DCFPyL. As the predictive power of in vitro stability assays is limited (*25*), the metabolic stability of the candidates was

TABLE 2
Tracer Uptake (SUV_{BW}) in Different Tissues 60–120 Minutes After Injection ($n = 3$ Each)

Tracer	SCG	Salivary gland	Liver	Blood	Bone	Background
^{18}F-DCFPyL	20.9 ± 8.2	13.2 ± 5.3	78.4 ± 29.4	12.9 ± 3.0	10.5 ± 3.5	3.2 ± 0.7
^{18}F-JK-PSMA-7	31.3 ± 10.5	14.4 ± 2.4	119.3 ± 8.3¶	16.3 ± 4.2	9.9 ± 1.9	4.0 ± 1.0
^{18}F-JK-PSMA-8	14.4 ± 2.6	9.0 ± 2.5	29.0 ± 7.2	8.6 ± 0.3	19.2 ± 2.1	3.2 ± 0.4
^{18}F-PSMA-1007	94.8 ± 19.6*	62.1 ± 14.2†	50.7 ± 4.3	62.6 ± 10.7‖	33.2 ± 9.5#	15.9 ± 1.7**
^{68}Ga-PSMA-11	41.0 ± 3.4	38.4 ± 10.2‡	43.7 ± 14.4	39.6 ± 4.6§	18.5 ± 0.6	9.2 ± 0.6**

*Significantly higher than any other ($F_{4,10} = 26.52$, $P < 0.0001$; post hoc $P < 0.05$).
†Significantly higher than any other ($F_{4,10} = 22.06$, $P < 0.0001$; post hoc $P < 0.05$).
‡Significantly higher than ^{18}F-DCFPyL ($F_{4,10} = 22.06$, $P < 0.0001$; post hoc $P < 0.05$).
¶Significantly higher than ^{18}F-JK-PSMA-8 (^{18}F-PSMA-1007 and ^{68}Ga-PSMA-11. $F_{4,10} = 7.83$, $P = 0.0040$; post hoc $P < 0.05$).
‖Significantly higher than any other ($F_{4,10} = 47.59$, $P < 0.0001$; post hoc $P < 0.05$).
§Significantly higher than ^{18}F-DCFPyL, ^{18}F-JK-PSMA-7, and ^{18}F-JK-PSMA-8 ($F_{4,10} = 47.59$, $P < 0.0001$; post hoc $P < 0.05$).
#Significantly higher than any other ($F_{4,10} = 12.19$, $P = 0.0007$; post hoc $P < 0.05$).
**Significantly different from all others ($F_{4,10} = 93.81$, $P < 0.0001$; post hoc $P < 0.05$).

determined in healthy rats. High stability toward in vivo defluorination is especially important for PCa imaging. ^{18}F-fluoride avidly accumulates not only in PCa bone lesions but also in healthy bones. This could lead to incorrect diagnosis and wrong therapy. PSMA-specific cellular accumulation of ^{18}F-JK-PSMA-9, ^{18}F-JK-PSMA-11, and ^{18}F-DCFPyL was comparable. In contrast, ^{18}F-JK-PSMA-7 revealed significantly higher accumulation rates. All 3 ligands were largely inert toward in vivo defluorination and were, together with ^{18}F-JK-PSMA-8, the closest structural analog of ^{18}F-JK-PSMA-7, chosen for further studies.

For the in vivo evaluation we used the rat peripheral ganglia as a model for small focal PSMA-positive lesions making use of their high PSMA expression and small size (2.5–3.5 mm), comparable, for example, to the size of small lymph nodes. We determined the TBR of the above-mentioned candidates in the SCG of rats. Only ^{18}F-JK-PSMA-7 had a TBR higher than that of ^{18}F-DCFPyL. Notably, the small structural difference between JK-PSMA-7 and -8 (methoxy substituent in either 4- or 2-position of the pyridine ring) resulted in different biodistribution. Also, introduction of the 4-ThiaLys (^{18}F-JK-PSMA-10) instead of the Lys residue (^{18}F-DCFPyL) resulted in a lower PSMA-specific cellular uptake in vitro and a low TBR in vivo.

Subsequently, we evaluated the biokinetics and biodistribution of ^{18}F-JK-PSMA-7 and -8, in comparison to ^{18}F-DCFPyL, ^{18}F-PSMA-1007, and ^{68}Ga-PSMA-11, in healthy rats. This study revealed a markedly high accumulation of ^{18}F-PSMA-1007 in PSMA-positive ganglia, but also in nontarget tissues such as neck muscles, blood and bones, compared with the other tracers. At the same time, liver uptake of ^{18}F-PSMA-1007 was low, indicating mainly renal elimination. Additionally, this tracer demonstrated significantly slower blood clearance. These differences may be explained by the presence of 2 acidic Glu residues leading to stronger electrostatic interactions of ^{18}F-PSMA-1007 with Lys- and Arg-rich proteins such as serum albumin (*26*). High blood protein binding should delay excretion of the tracer, resulting in lower accumulation in kidneys and bladder. This could be advantageous for detecting PCa metastases adjacent to the urethra and bladder. On the other hand, higher background radioactivity, especially in bone, could mask enrichment of the tracer in smaller lesions. Although liver uptake of ^{18}F-JK-PSMA-7 was higher than that of ^{18}F-DCFPyL, possibly because of the presence of the lipophilic methoxy group, liver uptake of the regioisomer ^{18}F-JK-PSMA-8 was significantly lower. We assumed that this apparent discrepancy could be explained by defluorination of ^{18}F-PSMA-8 in the liver, as indicated by radioactivity accumulation in bones.

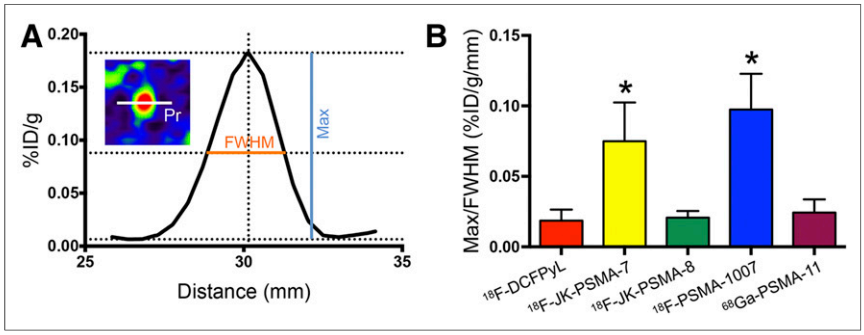

FIGURE 5. Acutance (measured for SCG) using different PSMA tracers. (A) Profile plot of 1-pixel profile (Pr in inset) through SCG center. Peak against adjacent background (max) and FWHM were measured. (B) Ratio max/FWHM roughly represents slope of profile plot and reflects acutance. *^{18}F-JK-PSMA-7 and ^{18}F-PSMA-1007 show significantly higher acutance than ^{18}F-DCFPyL, ^{18}F-JK-PSMA-8, or ^{68}Ga-PSMA-11 ($F_{4,10} = 12.77$, $P = 0.0006$; post hoc $P < 0.05$). %ID = percentage injected dose.

Image quality has the largest impact on the diagnostic accuracy of medical imaging, and TBR is widely used to compare different PET tracers. In contrast to ^{18}F-DCFPyL, ^{18}F-JK-PSMA-8, and ^{68}Ga-PSMA-11, the TBR for ^{18}F-JK-PSMA-7 significantly increased over time. The same effect, although less pronounced, was observed for ^{18}F-PSMA-1007. To explain these differences, we examined the time–activity curves of SCG and nontarget tissue in more detail. The initially high uptake of ^{18}F-DCFPyL, ^{18}F-JK-PSMA-8, and ^{68}Ga-PSMA-11 in the SCG decreased over time in accordance with the blood input function. This finding indicates a high amount of unbound tracer (*27*). In

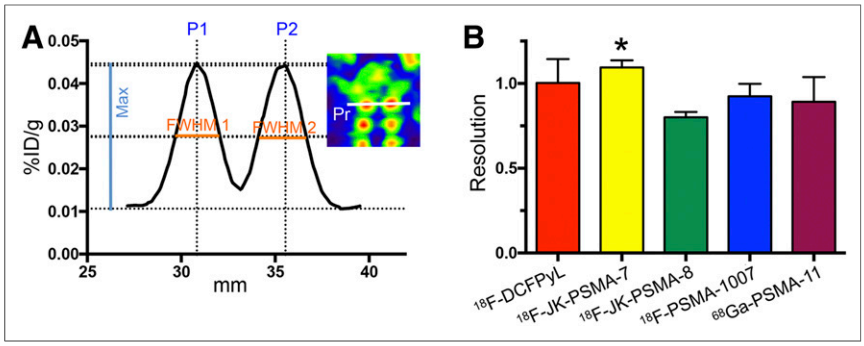

FIGURE 6. Resolution of images acquired with different tracers. (A) Profile plot of 1-pixel profile (Pr in inset) through apical pair of DRG. Peak against adjacent background (max) and FWHM were measured for each ganglion. P2–P1 was distance between peaks. (B) Formula R = 2(P2 − P1)/1.7(FWHM1 + FWHM2) yields image resolution. *Image resolution was significantly higher for ^{18}F-JK-PSMA-7 than for ^{18}F-JK-PSMA-8 ($F_{4,10}$ = 3.80, P = 0.0396; post hoc $P < 0.05$).

contrast, the time–activity curves of ^{18}F-JK-PSMA-7 and ^{18}F-PSMA-1007 decreased more slowly, and intersected the blood input function, finally reaching a plateau above blood radioactivity. This finding indicates active tracer–target binding and trapping (e.g., by internalization). For ^{18}F-PSMA-1007 and (to a lesser extent) ^{68}Ga-PSMA-11, however, a significantly longer retention of radioactivity in blood led to increased background activity.

Other important factors, such as resolution and acutance (edge contrast), have so far not been used for the qualitative assessment of PET images. High acutance increases the subjective perception of sharpness and allows improved measurements of lesion size. Acutance was significantly higher for ^{18}F-JK-PSMA-7 and ^{18}F-PSMA-1007 than for ^{18}F-DCFPyL, ^{18}F-JK-PSMA-8, and ^{68}Ga-PSMA-11. Resolution is the ability to delineate 2 small target tissues close to each other. ^{18}F-JK-PSMA-7 exhibited the highest resolution. It was slightly lower for ^{18}F-DCFPyL, ^{18}F-PSMA-1007, and ^{68}Ga-PSMA-11. Again, the resolution of ^{18}F-JK-PSMA-7 scans was significantly higher than that of ^{18}F-JK-PSMA-8 scans.

Among the evaluated ligands, ^{18}F-JK-PSMA-7 demonstrated the most favorable properties for imaging of PSMA-positive tissues. Because of the excellent preclinical imaging properties of ^{18}F-JK-PSMA-7, the first observational study on ^{18}F-JK-PSMA-7 PET/CT in patients with biochemical recurrence was initiated. This study suggests promising performance with regard to detection of PSMA-positive tumor tissue. These clinical and dosimetry data were preliminarily presented at the 2018 annual meeting of the Society of Nuclear Medicine and Molecular Imaging (*28,29*) and will be published in due course.

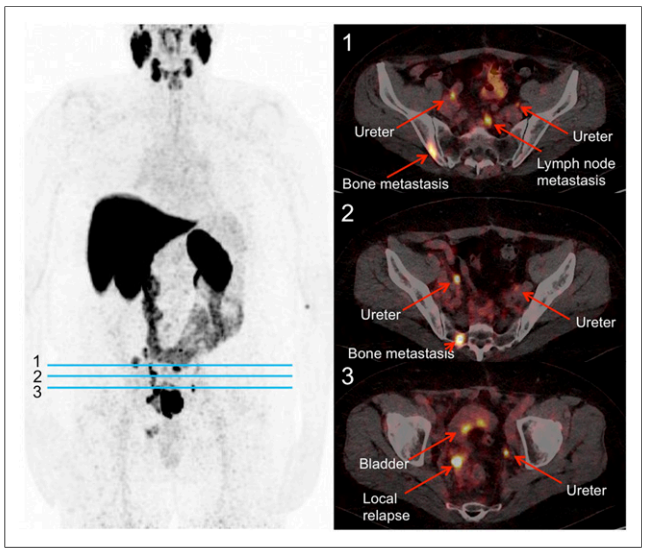

FIGURE 7. ^{18}F-JK-PSMA-7 scan in patient with relapsed PCa. This 64-y-old patient had serum prostate-specific antigen level of 130 ng/mL. Scan was started 233 min after injection of 384 MBq of ^{18}F-JK-PSMA-7. (Left) Maximum-intensity projection of PET image. (Right) PET/CT images at transverse levels indicated by blue lines.

CONCLUSION

The novel modular production protocol enabled the fast and high-yielding preparation of structurally different PSMA ligands. Application of peripheral ganglia of healthy rats as models of small PSMA-positive lesions allowed fast, precise, and cost-effective preclinical screening of PSMA-specific PET ligands. In the direct comparison with the already established PET tracers ^{68}Ga-PSMA-11, ^{18}F-DCFPyL, and ^{18}F-PSMA-1007, the novel probe, ^{18}F-JK-PSMA-7, in contrast to the regioisomeric ^{18}F-JK-PSMA-8, demonstrated favorable properties with respect to image quality and sensitivity to detect small PSMA-positive tissues. Accordingly, careful preclinical and clinical evaluations of ^{18}F-JK-PSMA-7 are under way.

DISCLOSURE

This study was funded by the LeitmarktAgentur.NRW and the European Regional Development Fund (LS-1-2-023c/EFRE-0800973 and LS-1-2-023b/EFRE-0800992). ^{18}F-JK-PSMA-7 is the subject of a patent application by Boris Zlatopolskiy, Philipp Krapf, Raphael Richarz, Alexander Drzezga, and Bernd Neumaier. No other potential conflict of interest relevant to this article was reported.

ACKNOWLEDGMENTS

We thank Dr. Agnieszka Morgenroth, RWTH Aachen, and Gordon Winter, University Clinic Ulm, for providing the LNCaP C4-2 cells; Marco Müller, ABX GmbH, Radeberg, for providing the PSMA-1007 and its precursor; and Austin Craig for proofreading the manuscript.

REFERENCES

1. Ross JS, Sheehan CE, Fisher HA, et al. Correlation of primary tumor prostate-specific membrane antigen expression with disease recurrence in prostate cancer. *Clin Cancer Res.* 2003;9:6357–6362.
2. Afshar-Oromieh A, Holland-Letz T, Giesel FL, et al. Diagnostic performance of ^{68}Ga-PSMA-11 (HBED-CC) PET/CT in patients with recurrent prostate cancer: evaluation in 1007 patients. *Eur J Nucl Med Mol Imaging.* 2017;44:1258–1268.
3. Chen Y, Pullambhatla M, Foss CA, et al. 2-(3-{1-carboxy-5-[(6-[^{18}F]fluoro-pyridine-3-carbonyl)-amino]-pentyl}-ureido)-pentanedioic acid, [^{18}F]DCFPyL, a PSMA-based PET imaging agent for prostate cancer. *Clin Cancer Res.* 2011;17:7645–7653.

4. Szabo Z, Mena E, Rowe SP, et al. Initial evaluation of [^{18}F]DCFPyL for prostate-specific membrane antigen (PSMA)-targeted PET imaging of prostate cancer. *Mol Imaging Biol.* 2015;17:565–574.
5. Rowe SP, Mana-Ay M, Javadi MS, et al. PSMA-based detection of prostate cancer bone lesions with ^{18}F-DCFPyL PET/CT: a sensitive alternative to ^{99m}Tc-MDP bone scan and Na^{18}F PET/CT? *Clin Genitourin Cancer.* 2016;14:e115–e118.
6. Rowe SP, Gorin MA, Hammers HJ, Pomper MG, Allaf ME, Javadi MS. Detection of ^{18}F-FDG PET/CT occult lesions with ^{18}F-DCFPyL PET/CT in a patient with metastatic renal cell carcinoma. *Clin Nucl Med.* 2016;41:83–85.
7. Dietlein F, Kobe C, Neubauer S, et al. PSA-stratified performance of ^{18}F- and ^{68}Ga-PSMA PET in patients with biochemical recurrence of prostate cancer. *J Nucl Med.* 2017;58:947–952.
8. Li X, Rowe SP, Leal JP, et al. Semiquantitative parameters in PSMA-targeted PET imaging with ^{18}F-DCFPyL: variability in normal-organ uptake. *J Nucl Med.* 2017;58:942–946.
9. Wondergem M, van der Zant FM, Knol RJJ, Lazarenko SV, Pruim J, de Jong IJ. ^{18}F-DCFPyL PET/CT in the detection of prostate cancer at 60 and 120 minutes: detection rate, image quality, activity kinetics, and biodistribution. *J Nucl Med.* 2017;58:1797–1804.
10. Dietlein M, Kobe C, Kuhnert G, et al. Comparison of [^{18}F]DCFPyL and [^{68}Ga]Ga-PSMA-HBED-CC for PSMA-PET imaging in patients with relapsed prostate cancer. *Mol Imaging Biol.* 2015;17:575–584.
11. Eder M, Neels O, Müller M, et al. Novel preclinical and radiopharmaceutical aspects of [^{68}Ga]Ga-PSMA-HBED-CC: a new PET tracer for imaging of prostate cancer. *Pharmaceuticals (Basel).* 2014;7:779–796.
12. Cardinale J, Martin R, Remde Y, et al. Procedures for the GMP-compliant production and quality control of [^{18}F]PSMA-1007: a next generation radiofluorinated tracer for the detection of prostate cancer. *Pharmaceuticals (Basel).* 2017;10:77.
13. Richarz R, Krapf P, Zarrad F, Urusova EA, Neumaier B, Zlatopolskiy BD. Neither azeotropic drying, nor base nor other additives: a minimalist approach to ^{18}F-labeling. *Org Biomol Chem.* 2014;12:8094–8099.
14. Neumaier B, Zlatopolskiy BD, Richarz R, Krapf P. Method for the production of ^{18}F-labeled active esters and their application exemplified by the preparation of a PSMA-specific PET-tracer. *Patent WO2016030329A1.* 2014.
15. Bouvet V, Wuest M, Jans HS, et al. Automated synthesis of [^{18}F]DCFPyL via direct radiofluorination and validation in preclinical prostate cancer models. *EJNMMI Res.* 2016;6:40.
16. Ravert HT, Holt DP, Chen Y, et al. An improved synthesis of the radiolabeled prostate-specific membrane antigen inhibitor, [^{18}F]DCFPyL. *J Labelled Comp Radiopharm.* 2016;59:439–450.
17. Krapf P, Richarz R, Urusova EA, Neumaier B, Zlatopolskiy BD. Seyferth-Gilbert homologation as a route to ^{18}F-labeled building blocks: preparation of radiofluorinated phenylacetylenes and their application in PET chemistry. *Eur J Org Chem.* 2016;3:430–433.
18. Drennen B, Scheenstra JA, Yap JL, et al. Structural re-engineering of the alpha-helix mimetic JY-1-106 into small molecules: disruption of the Mcl-1-Bak-BH3 protein-protein interaction with 2,6-di-substituted nicotinates. *ChemMedChem.* 2016;11:827–833.
19. Ehara T, Irie O, Kosaka T, et al. Structure-based design of substituted piperidines as a new class of highly efficacious oral direct renin inhibitors. *ACS Med Chem Lett.* 2014;5:787–792.
20. Gajera JM, Gharat LA, Kattige VG, Khairatkar-Joshi N, Narayana L, inventors. Glenmark Pharmaceuticals S.A., assignee. Tricyclic compounds as mPGES-1 inhibitors. Patent WO2012110860A1. October 17, 2013.
21. Kim DW, Jeong HJ, Lim ST, Sohn MH. Tetrabutylammonium tetra(tert-butyl alcohol)-coordinated fluoride as a facile fluoride source. *Angew Chem Int Ed Engl.* 2008;47:8404–8406.
22. Murelli RP, Zhang AX, Michel J, Jorgensen WL, Spiegel DA. Chemical control over immune recognition: a class of antibody-recruiting small molecules that target prostate cancer. *J Am Chem Soc.* 2009;131:17090–17092.
23. Qi J, Leahy RM, Cherry SR, Chatziioannou A, Farquhar TH. High-resolution 3D Bayesian image reconstruction using the microPET small-animal scanner. *Phys Med Biol.* 1998;43:1001–1013.
24. Dolan JW. Peak tailing and resolution. *LC GC Eur.* 2002;15:334–337.
25. Zlatopolskiy BD, Zischler J, Schafer D, et al. Discovery of 7-[^{18}F]fluorotryptophan as a novel positron emission tomography (PET) probe for the visualization of tryptophan metabolism in vivo. *J Med Chem.* 2018;61:189–206.
26. Kragh-Hansen U, Chuang VT, Otagiri M. Practical aspects of the ligand-binding and enzymatic properties of human serum albumin. *Biol Pharm Bull.* 2002;25:695–704.
27. Morris ED, Lucas MV, Petrulli JR, Cosgrove KP. How to design PET experiments to study neurochemistry: application to alcoholism. *Yale J Biol Med.* 2014;87:33–54.
28. Hohberg M, Dietlein M, Kobe C, et al. Biodistribution and radiation dosimetry of the novel ^{18}F-labeled prostate-specific membrane antigen-ligand PSMA-7 for PET/CT in prostate cancer patients [abstract]. *J Nucl Med.* 2018;59(suppl 1):88.
29. Dietlein M, Hohberg M, Kobe C, et al. Performance of the novel ^{18}F-labeled prostate-specific membrane antigen-ligand PSMA-7 for PET/CT in prostate cancer patients. *J Nucl Med.* 2018;59(suppl 1):452.